Bulletin of the JSME Vol.12, No.1, 2018
Journal of Advanced Mechanical Design, Systems, and Manufacturing

Ultraprecision cutting of single-crystal calcium fluoride for fabricating micro flow cells

Ryo KOMIYA*, Tetsunari KIMURA**,***,****, Takashi NOMURA**,
Minoru KUBO**,*** and Jiwang YAN*
* Department of Mechanical Engineering, Faculty of Science and Technology, Keio University
Hiyoshi 3-14-1, Kohoku-ku, Yokohama 223-8522, Japan
E-mail: yan@mech.keio.ac.jp
**RIKEN, SPring-8 Center, 1-1-1 Kouto, Sayo-cho, Sayo-gun, Hyogo 679-5148, Japan
***JST PRESTO, 4-1-8 Honcho, Kawaguchi, Saitama 332-0012, Japan
****Present address: Department of Chemistry, Graduate School of Science, Kobe University
1-1 Rokkodai-cho, Kobe, Hyogo 657-8501, Japan

Received: 3 August 2017; Revised: 16 December 2017; Accepted: 26 January 2018

Abstract
Single-crystal infrared (IR) spectroscopy is a promising method for protein structure analysis, where a protein crystal sample is fixed in a micro flow cell. Single-crystal calcium fluoride (CaF_2) is expected as the flow cell substrate material for its excellent optical property. However, CaF_2 is a highly brittle material having strong anisotropy, thus is extremely difficult to machine. Up to date, there is no available literature on fabrication of CaF_2 flow cells. In this study, micro flow cells of single-crystal CaF_2 were fabricated by ultraprecision cutting technology. Fly cutting was conducted using a single-crystal diamond tool having straight edges to generate a depth-varying rectangle cross section for the flow cell. The effects of cutting direction, workpiece orientation, undeformed chip thickness and tool rake angle on cutting behavior were investigated. Based on experiments and analysis, optimal conditions for ductile machining of micro grooves in CaF_2 were identified. As a result, a 10 μm deep CaF_2 micro flow cell with surface roughness of 2.4 nmRa was successfully fabricated. Using the fabricated flow cell, IR spectroscopic analysis of a protein single crystal at room temperature was succeeded. This study demonstrated the effectiveness of ultraprecision cutting technology in CaF_2 micro flow cell fabrication, which contributes to the IR analysis of protein, and in turn, the advance of life science.

Keywords : Ultraprecision cutting, Single crystal, Calcium fluoride, Ductile machining, Micro flow cell

1. Introduction

Physiological processes are series of chemical reactions regulated by proteins. Protein structure analysis is important for revealing the functional mechanism of a protein at the atomic level. Conventionally, X-ray crystallography has been used for determining the atomic arrangement of a protein, whereas infrared (IR) spectroscopy is available for analyzing the chemical structure and reactivity of functional sites in the protein. Recently, Kubo et al. developed a highly-sensitive IR spectrometer, suitable for measuring protein solution (Kubo et al., 2013). On the other hand, to facilitate the complementary use of IR and X-ray crystallographic analyses, the IR measurement for protein crystals is also desirable. Previously, an IR flow cell for mounting protein crystals has been reported, where a tapered Teflon spacer was custom-designed (Sage 1997). However, because the precise taper cutting of a thin Teflon sheet is very difficult, an alternative method for the crystal sample mounting still needs to be developed. In the IR analysis of protein, conventional plastic or glass micro flow cells cannot be used due to their low transmittance of IR light. Instead, a micro flow cell made of single-crystal calcium fluoride (CaF_2) is preferential for mounting the protein sample, because CaF_2 has excellent transmittance of IR light and enables precise IR measurements of proteins.

Conventional plastic and glass flow cells are made by chemical etching or injection/press molding methods. However, those methods are not applicable to single-crystal CaF_2. As an alternative approach, cutting technology is adopted in this study to fabricate CaF_2 micro flow cells. However, CaF_2 is a highly brittle material and very difficult to machine. In

Paper No.17-00388
[DOI: 10.1299/jamdsm.2018jamdsm0021]

diamond turning of CaF_2, surface microfracture is extremely easy to occur, and the cutting characteristics change strongly with the crystal planes of the workpiece due to its material anisotropy (Yan et al., 2004a). Ductile machining of CaF_2 is only possible when no thermal shock occurs and the undeformed chip thickness is smaller than a critical value which ranges from a few tens to several hundreds of nanometers (Yan et al., 2004b).

In this study, to fabricate a micro-flow cell which has a depth-varying rectangle cross section, fly cutting of CaF_2 was conducted using a single-crystal diamond tool with straight edges. Because the transmittance of CaF_2 depends on its surface roughness (Retherford et al., 2001), it is required that the surface roughness of the fabricated micro flow cell is in the nanometer level, without crack generation. To achieve this goal, the effects of cutting direction, undeformed chip thickness and tool rake angle on the cutting behavior were investigated. Based on the experimental results and analysis, optimal cutting conditions were identified and used for fabrication of CaF_2 flow cells.

2. Design of micro flow cell

Conventionally, protein crystal samples have to be frozen or dissolved in water for IR analysis because if water surrounding the protein evaporates at room temperature, the protein crystal structure will be damaged. However, if the protein crystals are frozen or dissolved, it is difficult to obtain the IR spectra precisely. In this study, a CaF_2 flow cell was designed to enable analysis of protein crystals at room temperature without freezing or dissolving the sample. The CaF_2 flow cell has two functions, namely, flowing water at a controlled speed, and capturing/fixing the protein crystal sample at a specific position precisely.

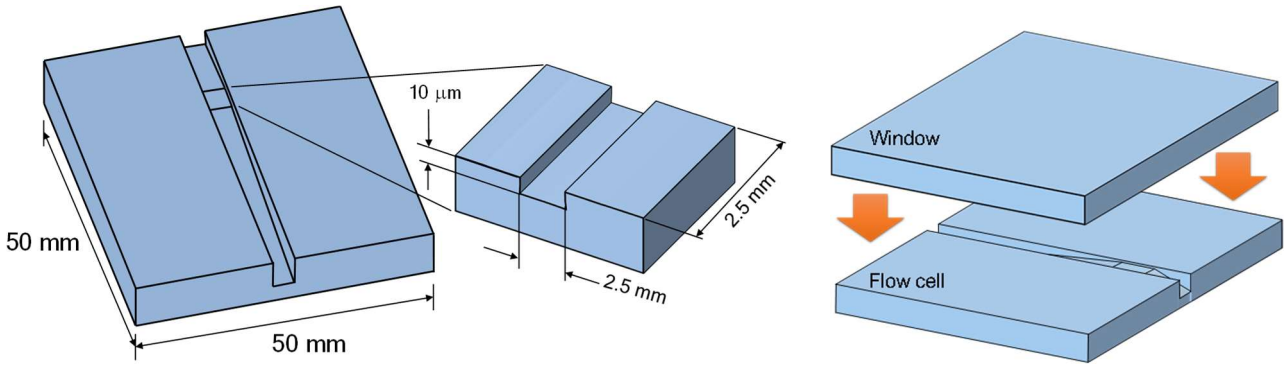

(a) Overall shape (b) Central region dimension (c) Flow cell assembly

Fig. 1 Schematic of designed flow cell

Figure 1 shows a typical example of micro flow cell design. The flow cell has two tapered long grooves connected by a flat shallow groove in the center, the depth, width and length of which are 10 μm, 2.5 mm, 2.5 mm, respectively. The size of protein crystal sample to be analyzed using the flow cell is in the range of 10 μm~100 μm, thus the protein sample will be fixed at a point where the groove depth is the same as the size of sample. CaF_2 (111) substrates, 50 mm square or 50 mm in diameter, with a thickness of 2.3 mm were used as the workpiece to fabricate the micro flow cell. To prevent water from evaporating, another piece of CaF_2 substrate, which has two polished flat surfaces, was used in the assembly as a window cover for the fabricated micro flow cell.

3. Cutting experiments

Crystalline materials such as silicon and germanium have anisotropy in mechanical properties, and thus the machining mechanism depends on cutting directions with respect to the crystal planes (Yan et al., 2004c, O'Connor et al., 2005). Single-crystal CaF_2 has a cubic structure, as shown in Fig. 2. The slip system of CaF_2 is $\{001\}\langle 1\bar{1}0\rangle$, and the cleavage plane is $\{111\}$. To find the best cutting direction, fundamental cutting experiments were performed along 12 different directions at an interval of 30° in the range of 0°~330° (clockwise) from the orientation flat (OF) $[1\bar{1}0]$ of the workpiece. In each cutting direction, a 10 μm deep groove was cut and the surface of the groove was characterized and compared.

A 5-axis ultraprecision machine tool ROBONANO α-0iB (FANUC Corporation), as shown in Fig. 3, was used for cutting experiments. Fly cutting method was adopted. A single-crystal diamond tool was rotated by the air bearing spindle

[DOI: 10.1299/jamdsm.2018jamdsm0021]

of the machine, and fed over the workpiece to cut grooves. The tool has a square tip, and the straight edge at the tool tip was 1 mm long. Figs. 4 (a) and (b) show schematics of two fly cutting operations: down cut and up cut, respectively. In down cut, the feed direction of workpiece is the same as the direction in which the tool moves, so that chip thickness decreases as the tool rotates. In up cut, the feed direction of workpiece is opposite to the direction in which the tool moves, thus chip thickness increases as tool rotates.

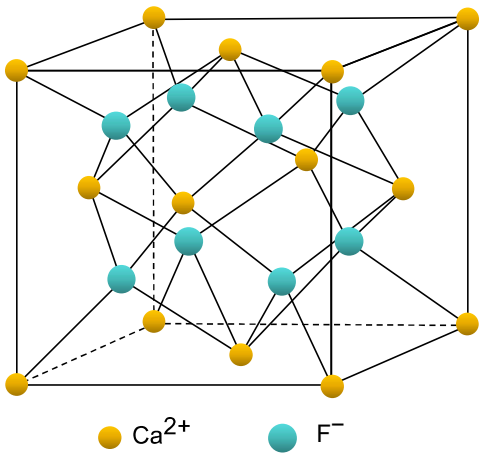

Fig. 2 Crystal structure of calcium fluoride

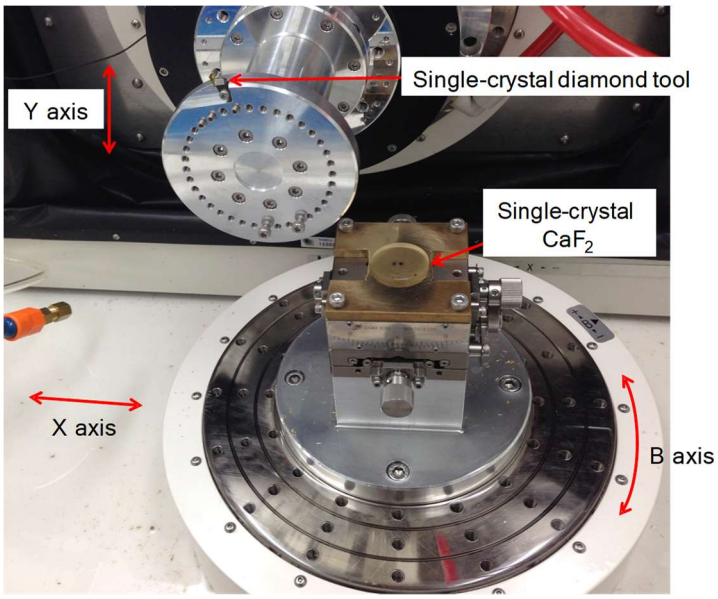

Fig. 3 Photograph of the main section of machine tool

For all cutting directions, down cuts and up cuts were performed to cut micro grooves with a depth of 10 μm at a maximum undeformed chip thickness of 200 nm. Two lengths were then measured using a laser-probe surface profilometer. One is length L, which is the total length of cut (including ductile- and brittle-cut regions); the other is length l, which is the length of brittle-cut region with crack generation. Using these parameters, the critical undeformed chip thickness h_c for brittle-to-ductile transition of cutting mode was calculated by the following equations:

$$\sin\theta_c = \frac{L-l}{R} \tag{1}$$

$$h_c = \frac{2\pi R V_w}{Z V_c} \sin\theta_c \tag{2}$$

where R is the radius of tool rotation, θ_c is the angle between the vertical direction and the line from center of rotation to ductile-brittle transition point, V_w is the feed of workpiece, V_c is the velocity of rotating tool, Z is the number of cutting edges.

[DOI: 10.1299/jamdsm.2018jamdsm0021]

In diamond turning of brittle materials, a negative tool rake angle enhances compressive stress in cutting region, and in turn, makes critical undeformed chip thickness larger (Leung et al., 1998, Yan et al., 2001). In this study, different tool rake angles 0°, -10°, -20° were used for cutting to find the best tool rake angle for flow cell fabrication.

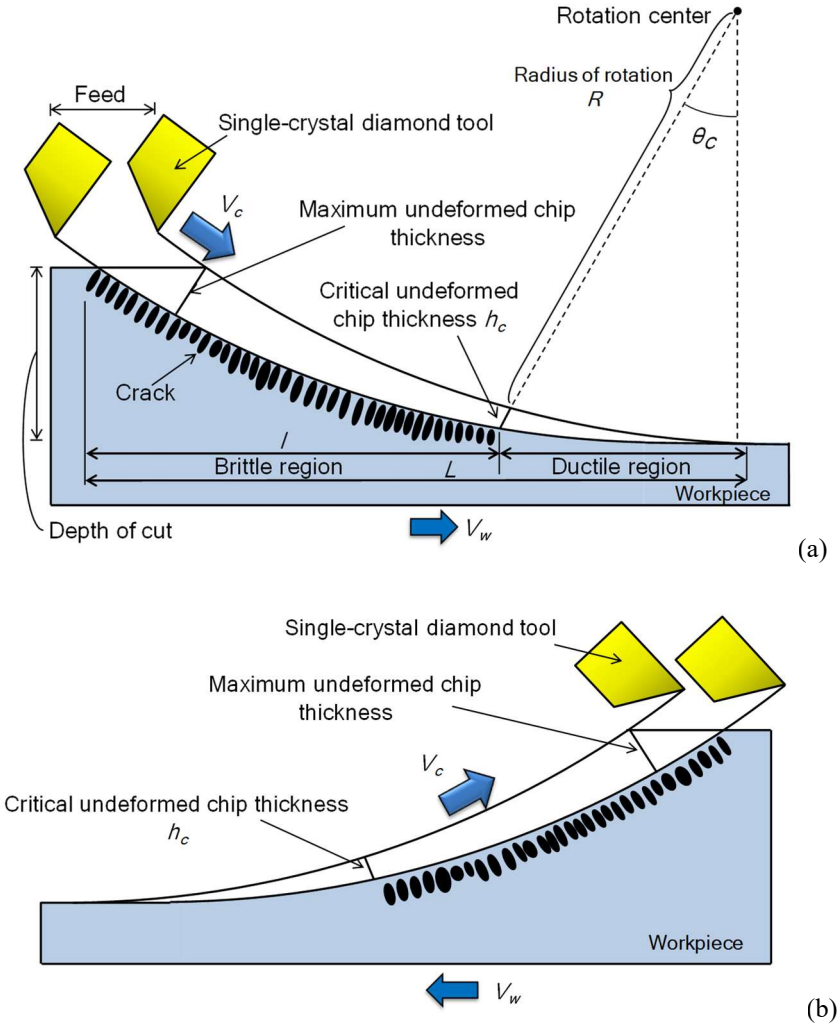

Fig. 4 Schematic diagrams of two kinds of fly cutting operation: (a) down cut, (b) up cut.

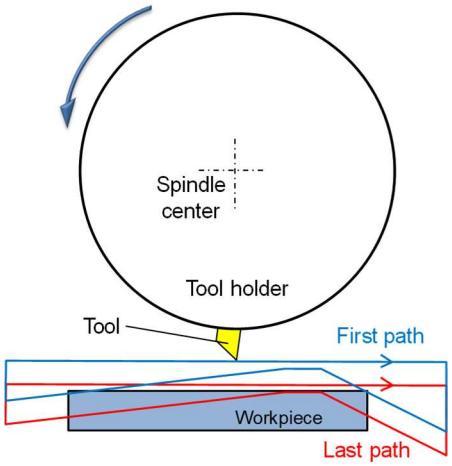

Fig. 5 Tool paths for fabricating micro flow cell

Fig. 5 shows the tool path used for cutting micro flow cell, which was controlled by a computer program. To generate the shape of the flow cell, rough cutting and fine cutting were performed by changing the tool feed rate and depth of cut.

[DOI: 10.1299/jamdsm.2018jamdsm0021]

As the largest depth of groove is 2.04 mm, totally 204 cutting cycles were performed, where the depth of cut for a single cutting cycle was 10 μm. The radius of the tool rotation was 440 mm.

4. Results and discussion

4.1 Effect of cutting direction

Figure 6 shows typical micrographs of workpiece surfaces machined along different directions by down cuts using a -20° rake angle tool. For 30° and 120°, from left to right, brittle-to-ductile transition is clearly identified. In this study, the brittle-to-ductile transition point is defined as the location where a micro crack bigger than 1 μm begins to occur. In Fig. 6, the brittle-cut region of 120° (930 μm) is longer than that of 30° (662 μm). In contrast, no micro cracks can be seen along 90°, and the entire surface is ductile cut. Figure 7 shows relationship between cutting directions and critical undeformed chip thickness which is obtained by measuring the length of the brittle region, as shown in Fig. 6. It is found that critical undeformed chip thickness changes roughly at a period of 120°. No cracks occur on the surfaces for cutting directions of 90°, 210°, and 330°, indicating that the critical undeformed chip thickness in these directions is bigger than the maximum undeformed chip thickness (200 nm) used in this experiment. In diamond turning of CaF_2 (111), the critical undeformed chip thickness in specific cutting directions reached 1200 nm [Yan et al, 2004b].

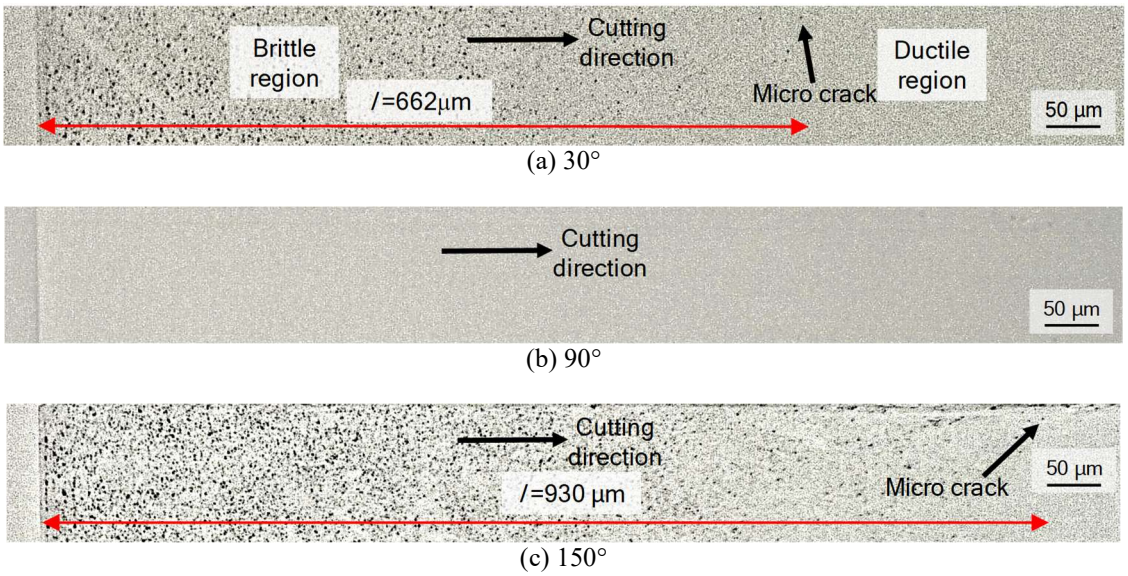

Fig. 6 Brittle-to-ductile transition in cutting mode along various cutting directions at down cuts (tool rake angle -20°)

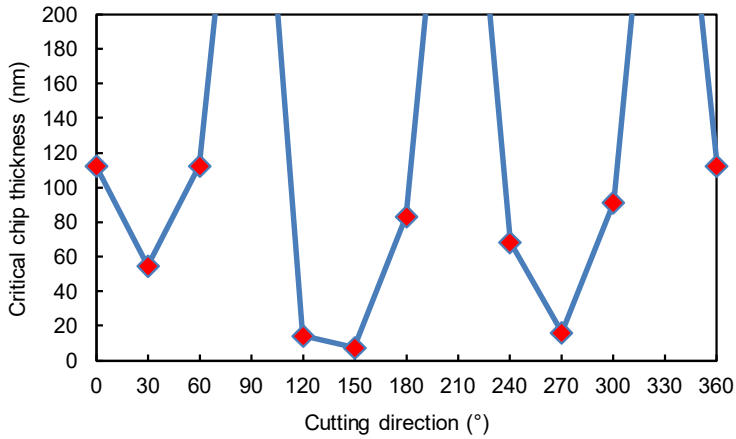

Fig. 7 Relationship between cutting direction and critical undeformed chip thickness at down cuts (tool rake angle -20°)

[DOI: 10.1299/jamdsm.2018jamdsm0021]

The strong anisotropy in brittle-to-ductile transition is caused by the orientation of slip planes in the CaF_2 crystal. It is possible to judge how easily slip happens in diamond turning by Schmid factor S_f which is defined as follows.

$$S_f = \cos\theta \cos\varnothing \tag{3}$$

where θ is the angle between cutting force F and vector vertical to slip plane, φ is the angle between cutting force F and vector parallel to slip direction. In this study, the change of Schmid factor in CaF_2 cutting was calculated by using the cutting force model proposed by Shibata eta al for single-crystal silicon (Shibata et al., 1996). The angle between cutting force direction and cutting direction is defined as α. In this study, the angle α was changed at an interval of 5° in the range of 0°~90° and the Schmid' factor of each slip plane was calculated for each α. It was shown that when α=20°, the calculation result agreed with the experimental results of Fig. 7. Thus, in the subsequent calculation, α=20° was used. This value is smaller than that of silicon cutting (α=65°) (Shibata et al., 1996). The difference might result from two aspects: one is that silicon cutting induces remarkably higher thrust forces than CaF_2, and the other is a higher negative rake angle (-40°) was used in silicon cutting.

The slip system of CaF_2 is $\{001\}\langle 1\bar{1}0\rangle$. There are totally 12 equivalent slip systems in CaF_2. Schmid factor was calculated in each slip system and the result is shown in Fig. 8, where α=20°. It is seen that the Schmid factors for cutting directions 90°, 210° and 330° are the biggest. There are 6 slip systems with the maximum Schmid factors in these cutting directions, which makes slip take place easily, whereas the other slip systems were inactive when two slip directions were symmetrical to the cutting direction (Shibata et al, 1996). This result agrees with the result of relationship between cutting direction and critical undeformed chip thickness shown in Fig. 7. The ductile/brittle response is also affected by the relative relationship between the cutting direction and the orientation of slip planes. For the 30° cutting direction, the slip plane $[1\bar{2}1]$ runs downwardly from the workpiece surface, leading to downward material flow inside workpiece, and in turn, causing severe subsurface damage. For the 90° cutting direction, however, the slip plane $[\bar{1}\bar{1}2]$ runs upwardly from the workpiece surface, where the deformed material will be removed together with chips, leaving less surface/subsurface damage.

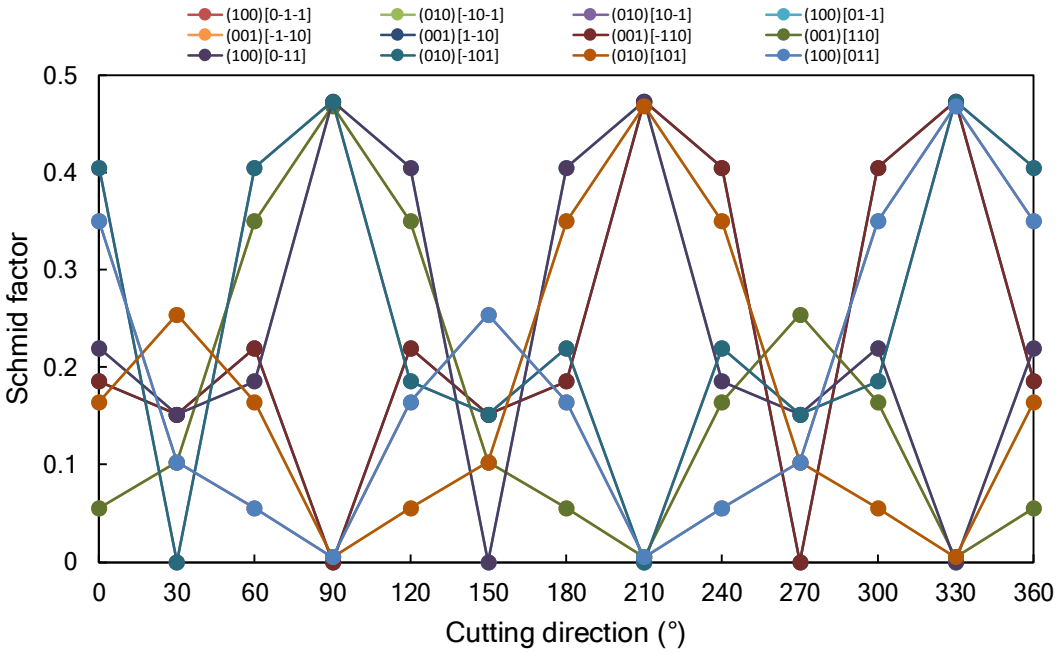

Fig. 8 Change of Schmid factor with cutting direction

[DOI: 10.1299/jamdsm.2018jamdsm0021]

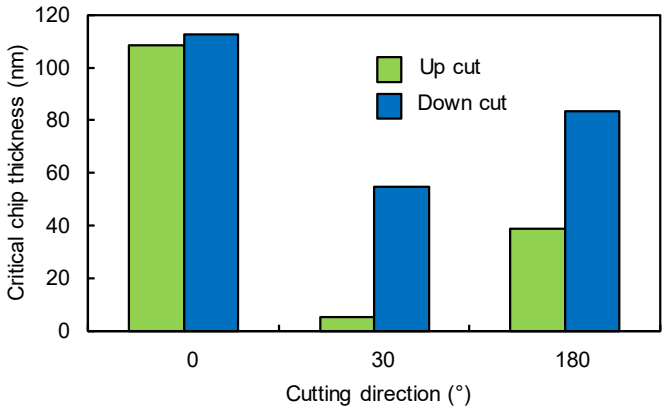

Fig. 9 Comparison of critical undeformed chip thickness for up/down cuts (tool rake angle of -20°)

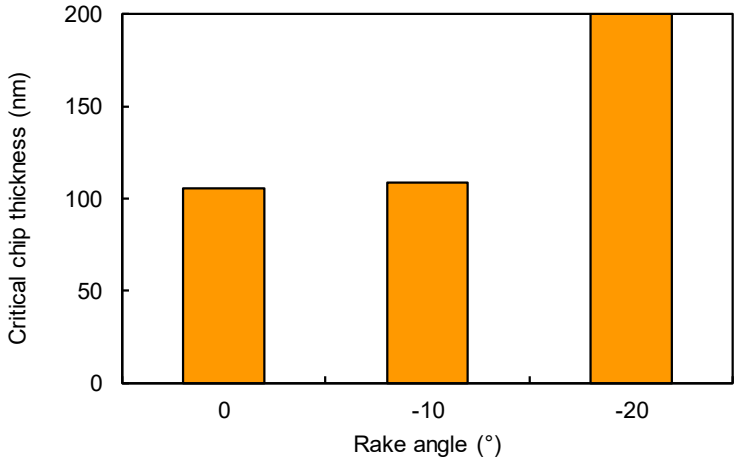

Fig. 10 Relationship between rake angle and critical undeformed chip thickness

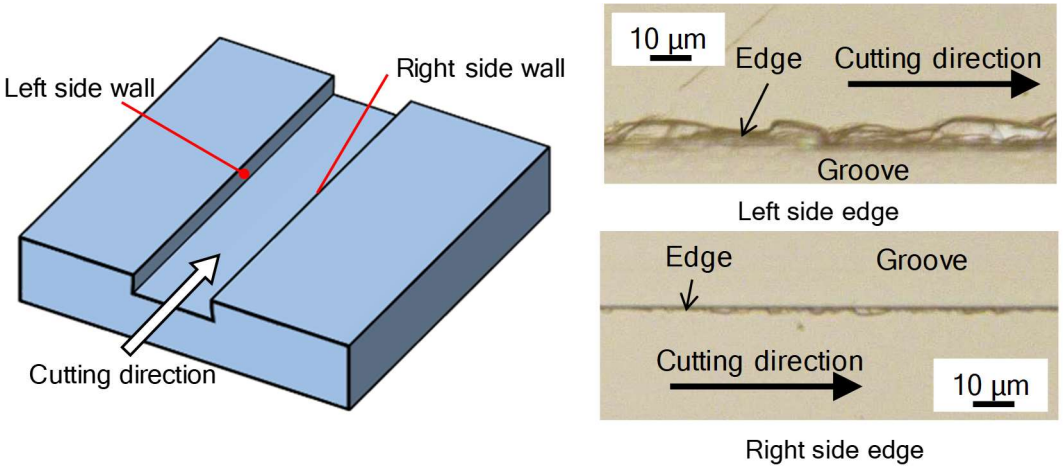

Fig. 11 Schematic and micrographs of two sides of groove edges along a cutting direction (0°)

4.2 Effect of up/down cut

Figure 9 shows a comparison of critical undeformed chip thickness for up/down cuts at a tool rake angle of -20°. In all these cutting directions, critical undeformed chip thickness is bigger in down cut than in up cut, indicating that ductile mode cutting can be realized more easily in down cuts than in up cuts. This result is different from that of glass cutting,

[DOI: 10.1299/jamdsm.2018jamdsm0021]

where up-cut results in a bigger critical undeformed chip thickness (Tamaki et al., 2005). This difference might be due to the lower mechanical strength of CaF_2 than glass (Azami et al., 2015). The tool-workpiece friction during the long ploughing region in up cuts causes tensile stress in the surface layer of CaF_2, as a result, more brittle fractures occur in the workpiece material.

4.3 Effect of tool rake angle

Figure 10 shows relationship between tool rake angle and critical undeformed chip thickness for down cuts at the 90° cutting direction. It is found that compared with 0° and -10°, ductile mode cutting can be realized most easily at a tool rake angle of -20°. When rake angle is -20°, no cracks were observed on the cut surface, indicating that critical undeformed chip thickness is bigger than maximum undeformed chip thickness (200 nm) set in the present experiment. This result is similar to the single-point diamond turning results of CaF_2 (Yan et al., 2004a, 2004b), where a -20° rake angle tool led to a maximum undeformed chip thickness of ~1200 nm along specific directions. As known from previous studies, a suitable negative tool rake angle induces hydrostatic stress field in front of tool edge, which reduces brittle fractures. However, an excessively high negative rake angle might cause severe strain in the surface layer and deep subsurface damage.

4.4 Groove edge chipping

It was found that micro chippings took place at groove edges under some conditions. Different from the groove bottom surfaces shown in Fig. 6 where the micro crack size is in the micron level, for the groove edges, however, chippings up to a few tens of microns take place. Figure 11 shows micrographs of the groove edges, left side and right side, especially, along 0° cutting direction using a -10° rake angle tool. It is clear that chippings on the left side ($(11\bar{2})$ plane) are bigger than those on the right side ($(\bar{1}\bar{1}2)$ plane). This trend was similar for other cutting directions of 0~90°. Then, the ImageJ software was used to process the micrographs and the total chipping area was obtained as shown in Fig. 12. The chipping area is slightly bigger in the cutting direction of 90°, but for all cutting directions, the chipping area of the left side wall is bigger than that of the right side wall.

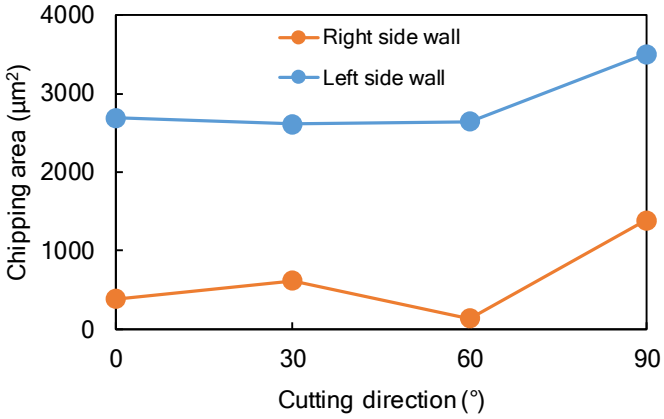

Fig. 12 Change of chipping areas for the two sides of groove edges along different cutting directions

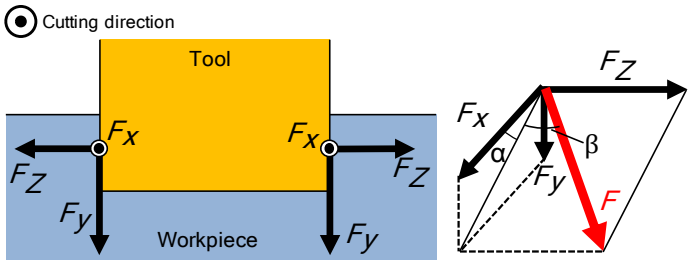

Fig. 13 Model of cutting forces at groove edges and definition of angles α and β

[DOI: 10.1299/jamdsm.2018jamdsm0021]

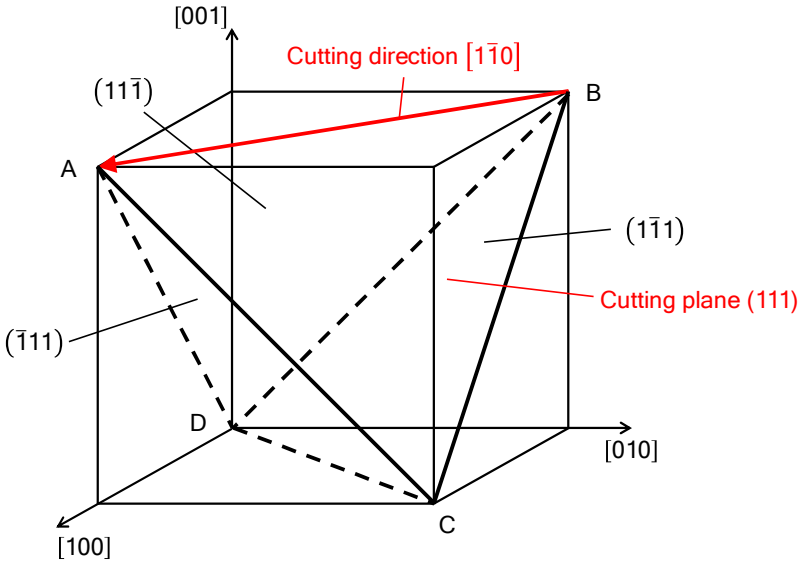

Fig. 14 Relationship between cutting direction and cleavage planes in CaF_2

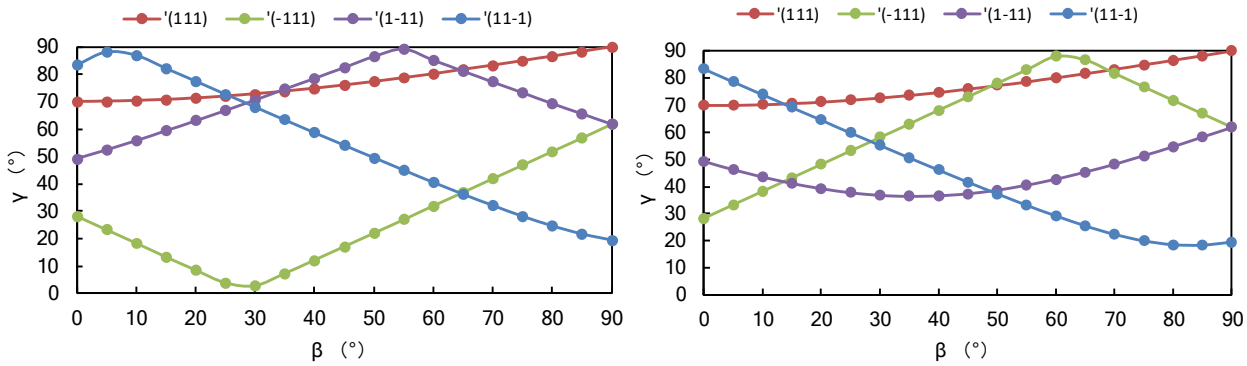

(a) Left side (b) Right side

Fig. 15 Relationship between β and γ

It is known that brittle fractures in crystal materials caused by cleavage, which happens when a tensile stress is applied vertically to a cleavage plane. Thus, the angle between the direction vertical to a cleavage plane and cutting force direction, which is defined as γ, is important for judging the easiness for cleavage fracture occurrence. As γ decreases, cleavage fractures happen more easily. In order to calculate γ, a three-dimensional force model for groove edge cutting was used, as shown in Fig. 13. In the figure, F_x, which is the cutting force along x axis, has the same value and direction on both sides; F_y, which is the cutting force along y axis, also has the same value and direction on both sides; F_z, which is the cutting force along z axis, has the same value but the opposite directions on both sides. To calculate γ, two angles α and β were defined to describe the relationship among F_x, F_y and F_z, as shown in Fig. 13. The values of α and β were changed at an interval of 5° in a range of 0°~90° and γ was calculated.

Single crystal CaF_2 has a cubic structure and the cleavage plane is {111}. As shown in Fig. 14, 4 equivalent planes (111) plane (ABC plane), (11$\bar{1}$) plane (ABD plane), ($\bar{1}$11)plane (ACD plane), and (1$\bar{1}$1) plane (BCD plane) are cleavage planes. In Fig. 14, the 0° cutting direction corresponds to $\overrightarrow{BA}$. The value of γ was calculated for each cleavage plane. Fig. 15 shows the change of γ with β when $\alpha = 20°$ for the 0° cutting direction. The minimum value of γ on the left side edge is 2.7°. In contrast, γ on the right side is approximately 20°, distinctly bigger than the left side. This explains that cleavage fractures happen more easily on left side edge than on right side edge.

To reduce groove edge chipping, it is important to use a small undeformed hip thickness to reduce the cutting forces. Figure 16 shows the change in chipping area with maximum undeformed chip thickness in cutting direction of 90° and 210° for the left side groove edge down-cut at a tool rake angle of -10°. As maximum undeformed chip thickness decreases, chipping area decreases too for both of the two directions. This means using a small maximum undeformed

[DOI: 10.1299/jamdsm.2018jamdsm0021]

chip thickness is essential to reduce edge chipping. As undeformed chip thickness decreases, the cutting force becomes smaller, and in turn, the size of tensile stress field decreases (Yan et al., 1999). This will suppress the initiation and propagation of cracks, especially around the sharp edges of a groove. It was noted that in Fig. 16 the area of chipping is different for the 90° and 210° cutting directions, though they are the same from the crystallographic viewpoints. This difference might be caused by the tool wear-induced edge geometry change for the diamond tool. Normally, a dull tool edge causes bigger edge chippings.

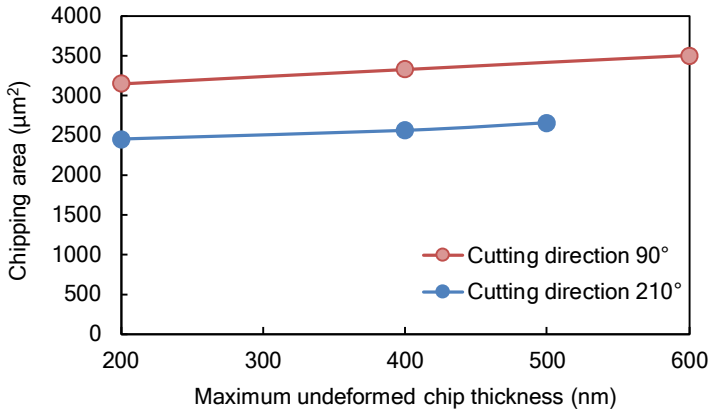

Fig. 16 Relationship between maximum undeformed chip thickness and chipping area (left side of groove)

4.5 Micro flow cell fabrication

Based on the comparison and analysis of fundamental cutting experiment results, a micro flow cell was test fabricated under selected conditions. A single-crystal CaF_2 (111) workpiece was used and the cutting direction was set to [1$\bar{1}$0]. Down cut was performed using a -20° rake angle tool at a spindle rotation rate of 2600 rpm. For the slope region, as groove edge quality is not strictly required, a high feed rate 48.8 mm/min was used at a depth of cut of 10 μm in rough machining to reduce cutting time, leading to a maximum undeformed chip thickness of 400 nm. For the 10 μm deep region, to reduce groove edge chipping, a lower feed rate was set (6.1 mm/min) and depth of cut was the same (10 μm). Thus, the maximum undeformed chip thickness was 50 nm, which enables completely ductile mode cutting.

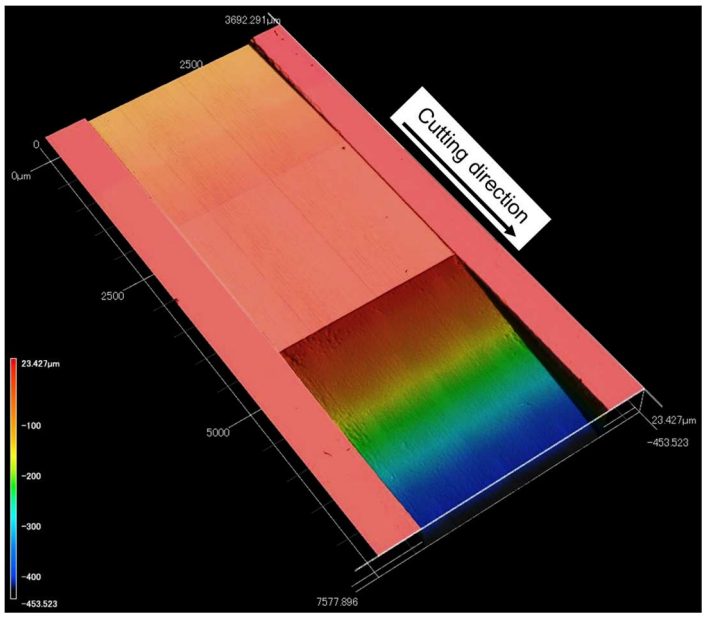

Fig. 17 Three-dimensional surface topography of the fabricated micro flow cell

[DOI: 10.1299/jamdsm.2018jamdsm0021]

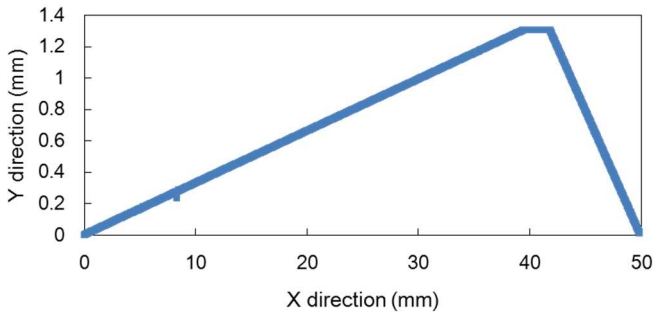

Fig. 18 Cross-sectional profile of the sloped groove bottom of fabricated micro flow cell

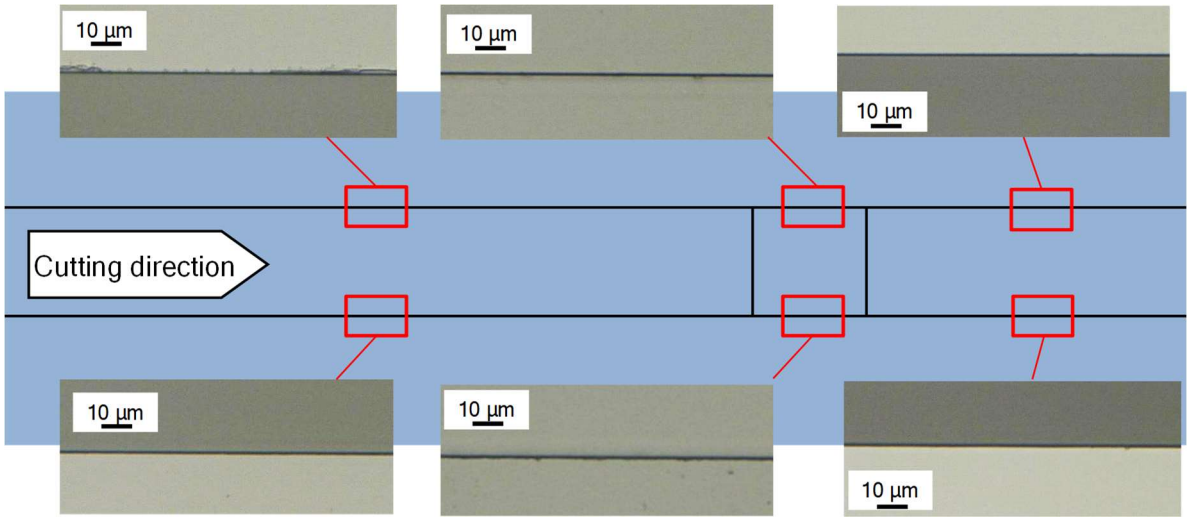

Fig. 19 Micrographs of groove edges at different locations of the fabricated flow cell

Figure 17 shows a three-dimensional surface topography of the fabricated micro flow cell measured by using a laser microscope. The flow cell surface is smooth and no fractures were detected, showing that ductile mode cutting was realized. The surface roughness of the groove bottom was 2.4 nmRa. This surface roughness enables good transparency of IR light and meets the requirements for proteins IR analysis. Fig. 18 shows a longitudinal cross-sectional profile of the flow cell. The sloped groove bottom was precisely generated. Figure 19 shows micrographs of groove edges of the fabricated micro flow cell at different locations. No apparent chipping was observed on the groove edge.

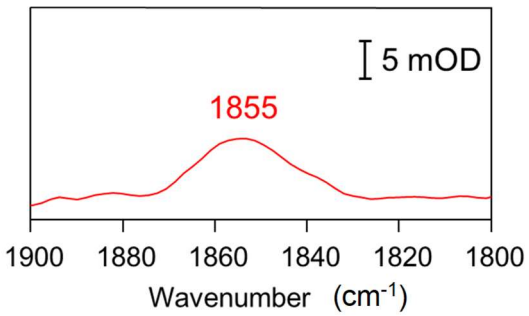

Fig. 20 IR spectrum of protein obtained by using the fabricated CaF_2 micro flow cell

Using the fabricated micro flow cell incorporated into a SPring-8/BL43IR micro-spectrometer, an IR spectrum of NO-bound P450nor was measured at 20°C, as shown in Fig. 20. P450nor is a heme protein that plays an important role in the nitrogen cycle on the earth by converting NO to N_2O. A large single crystal of P450nor (thickness ~20 µm) was used for the measurement under continuous flow of a NO-saturated buffer. The IR spectrum exhibits a clear peak at 1855 cm^{-1}, which arises from N-O stretching of the NO molecule bound at the heme. This result demonstrated that IR analysis of the protein crystal was successfully conducted at room temperature range without freezing by using the CaF_2 flow cell

[DOI: 10.1299/jamdsm.2018jamdsm0021]

fabricated in this study. This flow cell has been recently used in a further research of IR analysis of protein (Shimada et al., 2017), which is expected to contribute greatly to the advance of life science.

5. Conclusion

Single-crystal CaF_2 was machined by fly cutting using a single-crystal diamond tool on an ultraprecision machine tool, and conditions for ductile mode cutting were investigated. A micro flow cell for protein crystals analysis was successfully fabricated. The conclusions of this study are summarized as follows.

(1) When cutting direction is set to 90°, 210°, 330° from the orientation flat corresponding to $\langle 1\bar{1}0 \rangle$ direction, ductile mode cutting is realized more easily than other directions.
(2) A negative tool rake angle (-20°) is helpful for preventing microfractures.
(3) Down cut was better than up cut in terms of the ductile mode cutting performance.
(4) Micro chippings occur at the groove edges, the chipping size depending on crystal planes of groove side wall and undeformed chip thickness.
(5) A micro flow cell was fabricated by suppressing groove edge chipping. The surface roughness of the fly-cut flow cell surface was 2.4 nmRa, which meets the requirements for proteins analysis.
(6) The fabricated micro flow cell enabled IR measurement and analysis of protein crystals at 20℃, which have so far been difficult.

Acknowledgements

This research has been financially supported by the 34th research grant from the Machine Tool Engineering Foundation. The authors thank Dr. Y. Ikemoto for her technical support for the IR experiment at BL43IR of SPring-8 with the approval of JASRI (2015B1247).

References

Azami S., Kudo H., Mizumoto Y., Tanabe T., Yan J., Kakinuma Y., Experimental study of crystal anisotropy based on ultra-precision cylindrical turning of single-crystal calcium fluoride, Prec. Eng., Vol. 40, (2015), pp. 172-181.

Kubo M., Nakashima S., Yamaguchi S., Ogura T., Mochizuki M., Kang J., Tateno M., Shinzawa-Itoh K., Kato K., and Yoshikawa S., Effective pumping-proton collection facilitated by a copper site (Cu_B) of bovine heart cytochrome *c* oxidase, revealed by a newly developed time-resolved infrared system, J. Biol. Chem., Vol. 288, (2013), pp. 30259-30269.

Leung T. P., Lee W. B. and Lu X. M., Diamond turning of silicon substrates in ductile-regime, J. Mater. Proc. Tech., Vol. 73, (1998), pp. 42-48.

O'Connor B. P., M. Eric and Couey J. A., On the effect of crystallographic orientation on ductile material removal in silicon, Prec. Eng., Vol. 29, (2005), pp. 124-132.

Retherford R. S., Sabia R. and Sokira V. P., Effect of surface quality on transmission performance for (111) CaF_2, Appl. Surf. Sci., Vol. 183, (2001), pp. 264-269.

Sage, J. T., Infrared crystallography: structural refinement through spectroscopy, Appl. Spectro., Vol. 51, (1997), pp. 568-573.

Shibata T., Fujii S., Makino E. and Ikeda M., Ductile-regime turning mechanism of single-crystal silicon, Prec. Eng., Vol. 18, (1996), pp. 129-137.

Shimada A., Kubo M., Baba S., Yamashita K., Hirata K., Ueno G., Nomura T., Kimura T., Shinzawa-Itoh K., Baba J., Hatano K., Eto Y., Miyamoto A., Murakami H., Kumasaka T., Owada S., Tono K., Yabashi M., Yamaguchi Y., Yanagisawa S., Sakaguchi M., Ogura T., Komiya R., Yan J., Yamashita E., Yamamoto M., Ago H., Yoshikawa S., and Tsukihara T., A nanosecond time-resolved XFEL analysis of structural changes associated with CO release from cytochrome c oxidase, Sci. Adv., Vol. 3, No. 7 (2017), e1603042.

Tamaki J., Sato G., Maekawa K., Yan J., Kubo A., Effect of cutting edge shape of diamond abrasive grain on ductile mode grinding of optical glass - Measurement of critical depth of cut by means of single grit diamond cutting, J. Jap. Soc. Abras. Tech., Vol. 49, No. 6 (2005), pp. 335-340. (in Japanese).

Yan J., Tamaki J., Syoji K. and Kuriyagawa T., Single-point diamond turning of CaF_2 for nanometric surface, Int. J. Adv.

Manuf. Technol., Vol. 24, (2004a), pp. 640-646.

Yan J., Syoji K. and Tamaki J., Crystallographic effects in micro/nanomachining of single-crystal calcium fluoride, J. Vacuum Sci. Tech. B, Vol. 22, (2004b), pp. 46-51.

Yan J., Maekawa K., Tamaki J. and Kubo A., Experimental study on the ultraprecision ductile machinability of single-crystal germanium, JSME Int. J. (Series C), Vol. 47, No.1 (2004c), pp. 29-36.

Yan J., Syoji K. and Kuriyagawa T., Chip Morphology of Ultra-Precision Diamond Turning of Single Crystal Silicon, J. Jap. Soc. Prec. Eng., Vol. 65, No. 7 (1999), pp. 1008-1012. (in Japanese).

Yan J., Yoshino M., Kuriagawa T., Shirakashi T., Syoji K. and Komanduri R., On the Ductile Machining of Silicon for Micro Electro-mechanical Systems (MEMS), Opto-electronic and Optical Applications, Mater. Sci. Eng. A, Vol. 297, No. 1-2 (2001), pp. 230-234.

[DOI: 10.1299/jamdsm.2018jamdsm0021]